Available online at www.sciencedirect.com

ScienceDirect

Procedia CIRP 141 (2026) 556–561

www.elsevier.com/locate/procedia

10th Conference on High Performance Cutting (CIRP-HPC 2026)

Binder Jetting process chain optimization for M3 High-Speed tool steel

Marvin Dornick[a,*], Frederik Zanger[a]

[a]*Karlsruhe Institute of Technology (KIT), Kaiserstr. 12, 76131 Karlsruhe, Germany*

* Corresponding author. Tel.: +49-721-608-44288; fax: +49-721-608-45005. *E-mail address:* marvin.dornick@kit.edu

Abstract

The Binder Jetting (BJT) process expands material options and design freedom in powder metallurgy, enabling the processing of diverse materials, including high-speed steels (HSS), tungsten carbides, and ceramics. By producing near-net-shape geometries, it minimizes costly post-machining steps. While extensive research exists on how sintering temperature, holding time, atmosphere, and particle size distribution influence density, tensile strength, and hardness across materials and processes, for powder metallurgical processes and some additive processes, a comprehensive analysis of the entire Binder Jetting process chain and its key parameters for high-speed steel remains lacking. This study examined test specimens produced via Binder Jetting and sintered at different temperatures (1220 °C, 1230 °C, 1250 °C, 1270 °C) and holding times (4 and 8 hours). The resulting density and microstructure formation were then analyzed using metallographic analysis. Additionally, the influence of the sintering atmosphere was investigated, considering the chemical composition (argon, or nitrogen) and atmospheric pressure (1 or 100 bar). This study contributes to the optimization of the HSS-BJT process chain by presenting that, within the investigated range, higher sintering temperatures, atmospheric pressure and nitrogen atmosphere resulted in higher densities. The results also showed that density is influenced more by temperature than by holding time. Microstructure analyses and hardness measurements suggest that the desired properties of tools for metal cutting cannot be achieved through the used sintering routes. Therefore, alternative approaches are discussed.

Keywords: Binder Jetting; High-Speed Steel; BJT/M; Additive Manufacturing; Sintering.

1. Introduction

Conventional cutting tools are manufactured from high-speed steels (HSS), such as AISI M2 or M3, which are known for their high-temperature hardness. This property enables high cutting speeds and low wear, making hardness a key performance indicator for cutting tools [1,2].

Hardness is primarily determined by the microstructure, including iron-based phases, carbides, and grain size. In general, mechanical properties such as strength, ductility, and hardness are directly depended on the density. Consequently, for high-performance applications, especially in cutting operations, high densities are essential.

HSS are applied mostly as material for cutting tools for materials with low or moderate hardness. Since coatings can improve wear resistance of HSS it can also find application in cutting operations of harder materials, if the necessary tool geometry is complex or if the tool can be resharpened economically. Since HSS tools are usually tougher than carbide tools, they are also used in scenarios involving high impact or transverse forces.

Binder Jetting (BJT) is a promising technology for producing cutting tools in medium quantities, because it can be easily integrated into powder metallurgical (PM) process chains as alternative or substitution of conventional forming processes. It provides a high build rate, good scalability, and the general advantages of additive manufacturing (AM).

10.1016/j.procir.2026.03.036

Latter include reduced material waste, decreased machining effort and enhanced design flexibility. Therefore, BJT facilitates lightweight tool construction, functional integration, customized tools, and on-demand production without lead time, as it allows for cost-effective variations and simultaneous printing of multiple parts, as concluded in a comprehensive review on BJT by Mostafaei et al. 2021 [3].

However, the BJT process introduces additional challenges compared to conventional PM methods. Green parts produced via BJT typically show low densities (~50%) [3], whereas uniaxially or isostatically pressed PM parts reached up to 94% in density [4]. Since the mechanical properties depend on the sintered density, achieving high densities is crucial. However, this requires significant shrinkage, which can lead to distortion that is difficult to control. Multiple factors, including powder characteristics, binder properties, process parameters, and sintering conditions, influence the final material properties. Therefore, a deep understanding of the powder-binder system and optimized printing and sintering processes are essential.

No published studies yet exist on the effect of sintering atmospheres in manufacturing M2 or M3 HSS powders via the BJT process chain. Most research either focuses on single-stage AM processes (e.g., laser-based AM), which do not require sintering [5], or examines metal injection molding sintering [6-8]. As sintered properties result from many interdependent parameters that complexly influence each other, transfer from other materials onto HSS are strongly limited. Even a different particle size distribution (PSD) of a powder for a given material can influence parameters along the process chain drastically.

Only recently published studies sintered specimens produced via BJT:

In 2024, Anoop et al. examined the effect of heat treatment on the wear properties of M2-HSS. While the primary focus of the study was on the heat treatment subsequent to sintering and the evaluation of wear-related properties, no investigation was conducted into the effects of sintering atmosphere. Additionally, the chemical composition and pressure of the atmosphere were not addressed in the study [9].

In 2025, Choudhari et al. investigated the effects of sintering parameters on the wear behavior of M2 specimens. The application of an Argon atmosphere was conducted subsequent to an evacuation and debinding process, which was then followed by sintering in a single step. The sintering process was conducted within a temperature range of 1270 to 1300 °C for a duration of 1 to 2 hours. The cooling rates were varied, and a ball-on-disk test was performed to evaluate wear behavior. The density of the samples ranged from 90 to 96%, and it was found that a sintering temperature greater than 1270 °C resulted in significant grain growth and a shift from homogeneous carbide distribution to accumulation between grains [10].

In a previous study from 2024, said authors examined the effects of printing parameters, sintering temperature, and cooling rates on density and microstructure, as well as on hardness. The highest densities of 95% were achieved for specimens that were cooled in the furnace, and the lowest hardness of 510 to 620 HV [11] was recorded.

It is well established that nitrogen (N_2) atmospheres are known to be soluble in iron and to form hard nitrides with certain elements that are typically used in HSS alloys [4].

This study investigates the influence of a nitrogen sintering atmosphere compared to the usual inert argon atmosphere on the hardness and density of materials produced using BJT. The primary goal is to provide empirical data on how a nitrogen atmosphere, used as a soluble gas, affects hardness enhancement.

N_2 is hypothesized to not only inhibit oxidation more cost-effectively than argon but also to improve the hardness of HSS, making it more suitable for cutting applications.

The study further explores the impact of varying atmospheric pressures and different PSDs on the density and hardness of binder jetted components.

2. Materials and Methods

2.1. Powder Characterization

For this study a non-commercially available steel powder from BÖHLER brand, produced by voestalpine High Performance Metals Deutschland GmbH was used. An EDX measurement, following ASTM E2142 of the delivered powder showed the chemical composition in weight as 80.9% Fe, 6.3% W, 4.8% Mo, 4.4% Cr, 3.3% V and 0.4% Mn. According to DIN EN ISO 4957 the measured composition is fitting to HS6-5-3, also known as AISI M3 or SEL 1.3344, and is similar to BÖHLER s607, according to the content statement. Based on said content statement the carbon content is close to 1.2%.

For the experiments, powder in three states was used: original (R_0), once reused (R_1), and twice reused (R_2), all from the same batch and in the following color-coded depending on their state, in green (R_0), blue (R_1) and violet (R_2). The reusing process involved collecting the excess powder from a print job after cooling and removing the green part, then returning it to the wide-neck drum using desiccant silica bags to decrease atmospheric humidity to a minimum. As shown in Table 1, the PSD shifts slightly towards larger particles with each reusing cycle, a trend described before by Mirzababaei et al. [12] and confirmed by the presented data.

Table 1. PSD of used powders R_0, R_1, R_2 powder fraction deciles.

	R_0	R_1	R_2
D_{10} (μm)	20	21	21
D_{50} (μm)	41	43	45
D_{90} (μm)	81	83	85

2.2. Green Part Production using BJT

The specimens were produced on an Armadillo White BJT machine by CONCR3DE Printing B.V., with the print bed size reduced to 100 x 100 x 80 mm³. For efficient analysis cubes with the size of 10 x 10 x 10 mm³ were printed. The used parameters are presented in Table 2.

The solvent-based Metal Binder BM1001, designed for

metal AM by CONCR3DE Printing B.V., was used. No other external heat source, besides the IR heater was used during the process. To achieve suitable green part strength for depowdering, a subsequent binder curing process in a Memmert UF110 universal oven for 3 hours at 130 °C in air was applied. Subsequently, the cubes were depowdered using brushes and an industrial vacuum cleaner.

Table 2. Printing parameters for Binder Jetting green part production.

Parameter	Value	Unit
Layer height	100	µm
Feed height	120	µm
Droplet volume	52 x 10^{-12}	l
Powder Spread Velocity (Y)	41	mm/s
Roller Rotational Speed	2.5	s^{-1}
Velocity X & Y-Axis	138 (X), 168 (Y)	mm/s
Infrared Heater Intensity	100	%

2.3. Brown Part Production (Debinding)

The debinding profile was developed using thermogravimetric analysis, resulting in a two-step cycle. Below 180 °C, a heating rate of 300 K/h was applied, as no mass reduction and thus binder phase change was expected. For higher temperatures, the heating rate was reduced to 20 K/h to prevent sudden gas formation, which could cause structural defects. At 400 °C, heating was stopped, allowing the system to cool gradually.

The debinding was conducted using a Carbolite Gero GmbH & Co. KG GLO 10/11-1G annealing furnace to avoid contaminating the sintering furnace. To prevent oxidation, an argon (Ar) atmosphere was used.

2.4. Grey Part Production (Sintering Experiments)

For sintering the Carbolite Gero GmbH & Co. KG HTK 8 MO metal insulated chamber furnace was used, as N_2, H_2, Ar, combined atmospheres, and vacuum are supported. For each sintering experiment, six cubes were produced in the same batch using R_0, R_1, or R_2 powder.

The oven was brought to a near-vacuum atmospheric pressure to remove air from the part and the chamber before being flooded with the respective gas.

Table 3. Parameter variations from reference in BJT part process chain.

Parameter	Value		Unit	Symbol for **Variations**
	Reference	**Variation**		
Reusing	0	1 x reused, 2 x reused	-	**1, 2**
Temperature	1220	Sintering at 1230, 1250, 1270	°C	**30, 50, 70**
Pressure	P_∞ (~1)	Sintering at 100	bar	**100**
Atmosphere	Argon	Nitrogen, Argon while holding and Nitrogen while cool-down	-	**N, Nc**
Holding Time	4	Holding time at max. temperature for 8	h	**8**
Cooling Rate (as in Fig. 1)	3 steps (1-2-5)	rates 1, 2, 5 & maximal rate exponentially regressing from 70 to 2	°C/min	1 to 2 steps **2-5, 5, 10, 1-max, max**

As reference, the sintering temperature was set to 1220 °C, the sintering time to 4 hours, and the default sintering atmosphere to Ar. The cooling rate was based on the reversed heating steps, excluding holding times. The reference conditions furthermore included atmospheric pressure and original powder. All sintered variants are named adding the symbols in Table 3 for each applicable deviation from the reference values. For each sintering step 6 visually similar cubes were produced.

The heating rate of 5 K/min was maintained up to 700 °C, followed by a holding time of 1 hour, then increased at a rate of 2 K/min to 1000 °C and was held for 1 hour. Finally, the desired sintering temperature was approached with the rate of 1 K/min.

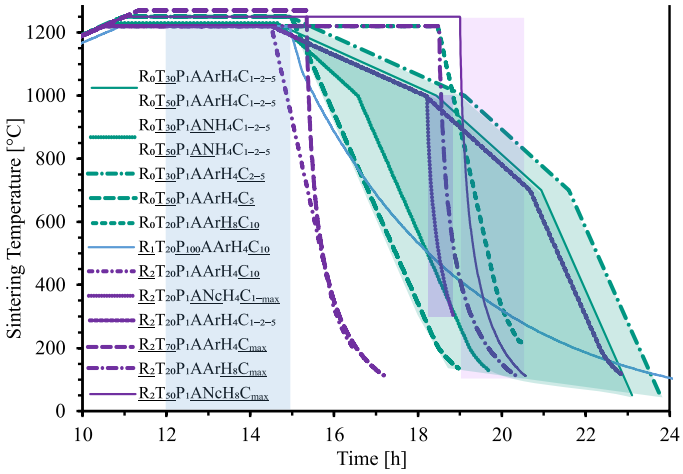

Fig. 1. Sintering profiles for measured oven temperature over time for different heat treatments.

The measured oven temperatures are visualized in Fig. 1. For pressurized sintering, hot isostatic pressing (HIP) was carried out at Fraunhofer IKTS Dresden and the time, when the pressure was held up, being highlighted as a transparent blue area.

As the furnace used continuous water cooling, cooling rates below than maximal rates required additional energy to achieve a controlled cooling.

2.5. Printed Part Characterization

For further characterization 3 cubes were embedded in a suitable resin for each sintering process. The characterization procedure contained a cutting step to the middle plane of the cube, to assess the bulk density, followed by a series of semi-automated wet grinding and polishing steps, according to ASTM E3-11 [13].

For density measurement of metal-AM parts, standardized methods include Archimedes and metallographic techniques, according to the ASTM guide F3637 as suitable methods [14]. The Archimedes method, is particularly suitable for low-porosity samples (<2% porosity). As the expected densities are partly far below 98% and even open porosity is expected, metallographic density estimation was employed as a validated alternative, as it

yields statistically equivalent results in bulk material. The embedded specimens were prepared by a series of fine wet grinding and polishing. Hereafter, 8 micrographs of the bulk with a magnification of 500 were analyzed using ImageJ for each 3 cubes per sintering experiment and statistically evaluated.

The hardness (HV1) of the resulting specimens was tested using the fully automated Vickers Micro Hardness Tester Qness 10 by ATM Qness GmbH, according to ASTM 384−22 [15]. For each sinter experiment the 3 cubes were tested and each was measured at 9 valid points.

Finally, to assess the microstructure of the material, the specimens were polished and etched with a mixture of 5 vol% nitric acid (HNO_3) in ethanol, according to ASTM E407–23 [16]. Subsequently, an assessment using light microscopy was performed.

3. Results

3.1. Microstructure

In Fig. 2(A) the metallographic microstructure of specimen $R_0T_{50}P_1A_NH_4C_{1\text{-}2\text{-}5}$ is presented exemplarily for specimens sintered in N_2 atmosphere. It cooled down slowly and blocky vanadium carbide (VC) and round molybdenum-tungsten carbide (M_6C) are visibly spread evenly. The fine line-like structures are identified as bainite (B) needles and the darker parts as pearlite (P). At the grain boundaries residual austenite (RA) was observed as light islands as well as the dark chromium nitride (CrN) in tubular shape.

In Fig. 2(B) an exemplary micrograph for the Ar-sintered, relatively fast cooled specimens is presented. The grain mainly consists of Perlite with Bainite between the grains.

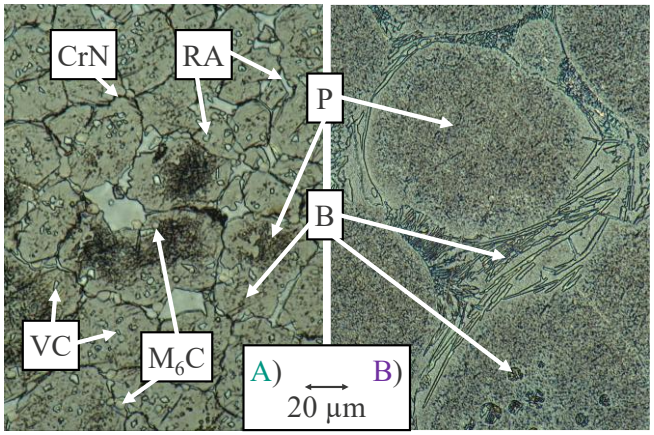

Fig. 2. Micrographs of grain structure of specimen $R_0T_{50}P_1A_NH_4C_{1\text{-}2\text{-}5}$ (A) and $R_2T_{70}P_1A_{Ar}H_4C_{max}$ (B) with marked microstructural features.

3.2. Density

The metallographically estimated densities of all sintered specimens are presented in Fig. 3, categorized by sintering temperature. The results reveal that densities exceeding 90% of the theoretical value were achieved exclusively when using the original powder, sintering at elevated temperatures (≥1250 C), or applying increased pressures.

A notable trend is the increasing variance in density with decreasing average density, with exceptions observed for samples $R_0T_{50}P_1A_{Ar}H_4C_5$ and $R_1T_{20}P_{100}A_{Ar}H_4C_{10}$. Near-full densities were attained only when sintering in a nitrogen atmosphere or under elevated pressure conditions.

Comparative analysis of specimens sintered at higher temperatures consistently demonstrates higher densities than those processed under otherwise identical conditions. For instance, a comparison between $R_0T_{20}P_1A_{Ar}H_8C_{10}$ and $R_2T_{20}P_1A_{Ar}H_8C_{max}$ indicates that minor shifts in PSD can result in a relative density difference of approximately 11%.

When either temperature or pressure is varied relative to the reference conditions ($R_2T_{20}P_1A_{Ar}H_4C_{10}$ vs. $R_1T_{20}P_{100}A_{Ar}H_4C_{10}$ and $R_2T_{70}P_1A_{Ar}H_4C_{max}$), increased pressure yields higher densities than elevated temperature.

Extended holding times ($R_2T_{20}P_1A_{Ar}H_8C_{max}$ vs. $R_2T_{20}P_1A_{Ar}H_4C_{10}$, C10H8 vs. $R_0T_{30}P_1A_{Ar}H_4C_{2\text{-}5}$, and $R_2T_{50}P_1A_{Nc}H_8C_{max}$ vs. $R_2T_{70}P_1A_{Ar}H_4C_{max}$) exhibit a lower, yet significant, positive effect on density when considering the combined effect of PSD, atmosphere, and temperature. An increase in cooling rate, as observed in samples sintered at 1230 °C and 1250 °C ($R_0T_{30}P_1A_{Ar}H_4C_{1\text{-}2\text{-}5}$ vs. $R_0T_{30}P_1A_{Ar}H_4C_{2\text{-}5}$ and $R_0T_{50}P_1A_{Ar}H_4C_{1\text{-}2\text{-}5}$ vs. $R_0T_{50}P_1A_{Ar}H_4C_5$), results in a reduced relative density. This effect is attributed to diminished heat intake (highlighted as green areas in Fig. 1), with the density difference becoming more pronounced at higher temperatures.

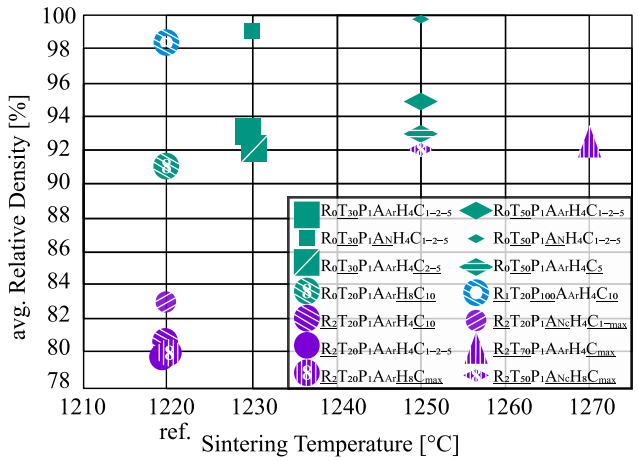

Fig. 3. Correlation between sintering temperature and relative density. Powder condition is coded as R_0 (green), R1 (blue) and R2 (violet), sintering atmosphere as size Ar (large), N_2 while cooling (medium) and N_2 (small), sintering temperature in shape as 1220 (●), 1230 (■), 1250(♦) and 1270(▲) in °C and cooling speed in °C/min as number of stripes with 1-2-5 ( ), 2-5 (/), 5 (=), 1-max (///), 10 (\\\\) and max (|||||). Experiments with increased holding time from 4 to 8 hours are marked with ‘8’and increase pressure from 1 to 100 bar is marked as a hollow symbol.

3.3. Hardness

The hardness values of the sintered specimens are presented in Fig. 4. The highest hardness values, exceeding 700 HV, were exclusively achieved in specimens sintered in a N_2-atmosphere ($R_0T_{30}P_1A_NH_4C_{1\text{-}2\text{-}5}$, $R_0T_{50}P_1A_NH_4C_{1\text{-}2\text{-}5}$ and $R_2T_{50}P_1A_{Nc}H_8C_{max}$), although substantial deviations were observed. However, this hardening effect was not evident in specimen $R_2T_{20}P_1A_{Nc}H_8C1\text{-}_{max}$.

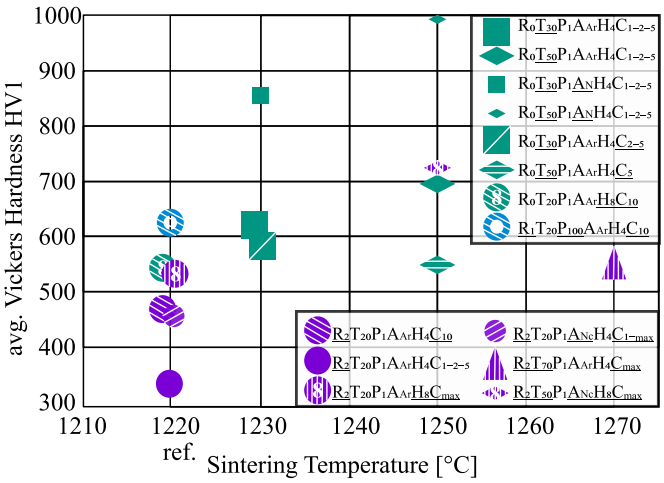

Fig. 4. Correlation between hardness and sintering temperature. Powder condition is coded as R_0 (green), R1 (blue) and R2 (violet), sintering atmosphere as size Ar (large), N_2 while cooling (medium) and N_2 (small), sintering temperature in shape as 1220 (●), 1230 (■), 1250(♦) and 1270(▲) in °C and cooling speed in °C/min as number of stripes with 1-2-5 ( ), 2-5 (/), 5 (=), 1-max (///), 10 (\\\\) and max (|||||). Experiments with increased holding time from 4 to 8 hours are marked with '8'and increase pressure from 1 to 100 bar is marked as a hollow symbol.

A slight trend toward higher hardness is observed for specimens with finer PSD. As density is known to influence mechanical parameters in general and hardness specifically [3] the trend is explainable by the higher densities observed. As illustrated in Fig. 5, a positive correlation between hardness and density is apparent, with a near-linear relationship for specimens produced from the original (i.e., finer) powder.

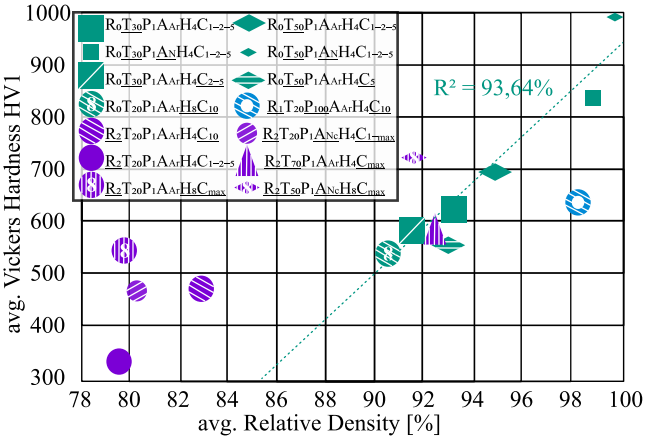

Fig. 5. Correlation between hardness and relative density. Powder condition is coded as R_0 (green), R1 (blue) and R2 (violet), sintering atmosphere as size Ar (large), N_2 while cooling (medium) and N_2 (small), sintering temperature in shape as 1220 (●), 1230 (■), 1250(♦) and 1270(▲) in °C and cooling speed in °C/min as number of stripes with 1-2-5 ( ), 2-5 (/), 5 (=), 1-max (///), 10 (\\\\) and max (|||||). Experiments with increased holding time from 4 to 8 hours are marked with '8'and increase pressure from 1 to 100 bar is marked as a hollow symbol. An apparent correlation for original powder is suggested, visualized via the dotted line.

A comparison between $R_0T_{20}P_1A_{Ar}\underline{H_8C_{10}}$ and $\underline{R_2}T_{20}P_1A_{Ar}\underline{H_8C_{max}}$ reveals that similar hardness values are achieved under comparable sintering conditions (1220 °C, 8 h), indicating that the cooling rate has an equivalent hardening effect to the increased density resulting from finer PSD. In Fig. 6 the higher density and the less extensive precipitations for $R_0T_{20}P_1A_{Ar}\underline{H_8C_{10}}$, become apparent and explain this observation.

Additionally, extended holding times exhibit a lesser influence on hardness compared to sintering temperature or atmosphere.

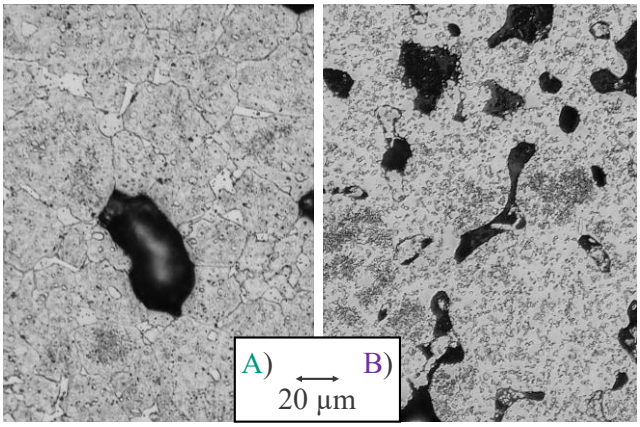

Fig. 6. A) Micrographs of grain structure of specimen $R_0T_{20}P_1A_{Ar}\underline{H_8C_{10}}$ and B) of specimen $\underline{R_2T_{70}}P_1A_{Ar}H_4\underline{C_{max}}$.

4. Discussion

The observation of density and hardness and the synthesis with the microstructure analysis allows for interpretation on the mechanisms that influence the resulting properties.

4.1. Influences of Sintering Parameters on Density

Sintering temperature is the most influential parameter affecting the resulting density, as it governs diffusion-driven densification processes. This is evident from the consistently higher densities achieved at elevated temperatures (≥1250 °C) compared to lower-temperature conditions (Fig. 3), confirming the dominant role of thermal activation in particle bonding and pore elimination.

However, increased pressure appears to exert a relatively stronger influence on density than temperature alone. Pressure reduces the mean center distances between particles and increases the contact surface area, thereby enhancing diffusion, particularly in specimens with reused powders and thus lower green part density. This effect is clearly demonstrated by the significantly higher densities observed in pressure-assisted sintering ($\underline{R_1}T_{20}\underline{P_{100}}A_{Ar}H_4\underline{C_{10}}$ vs. $R_0\underline{T_{50}}P_1A_{Ar}H_4\underline{C_5}$), where mechanical compaction augments densification more effectively than thermal activation alone.

4.2. Influences of Sintering Atmosphere on Density and Hardness

Sintering in a N_2-atmosphere yielded the highest densities (Fig. 3, near-full densification in $R_0\underline{T_{30}}P_1\underline{A_N}H_4C_{1\text{-}2\text{-}5}$ and $R_0\underline{T_{50}}P_1\underline{A_N}H_4C_{1\text{-}2\text{-}5}$) and hardness values over 700 HV (Fig. 4).

One key mechanism contributing to this effect is N_2 solubility in iron. Residual N_2 in pores reduces porosity, particularly at higher temperatures, where diffusion is accelerated. In contrast, Ar is inert and insoluble in iron and therefore hinders full densification by impeding diffusion-based pore elimination. This effect, known in PM [4], was observed as Ar-sintered specimens displayed lower densities (Fig. 3, e.g., Ar-sintered vs. N_2-sintered) and consequently, reduced hardness (Fig. 4) by mitigating the effect of reduced density on mechanical properties.

The other key mechanism is nitride formation, as evidenced by the drastic hardness increase (Fig. 4) and the micrographs. N_2 reacts with alloying elements (e.g., vanadium, chromium) forming hard nitrides (e.g., CrN), which significantly enhance hardness. The requirement for higher temperatures and extended holding times for nitride precipitation in $\underline{R_2T_{50}}P_1\underline{A_{Nc}H_8C_{max}}$ compared to $\underline{R_2}T_{20}P_1\underline{A_{Nc}}H_8\underline{C1\text{-}_{max}}$ further supports this conclusion.

It is plausible that, under N_2-atmosphere, both densification and nitride formation would have been further enhanced with extended holding times.

4.3. Impact of Cooling Rate on Microstructure and Hardness

Variations in cooling rate did not produce significant microstructural changes, as the dominant phases remained bainite and pearlite across all conditions. The reduction observed in hardness at higher cooling rates (Fig. 4) can be attributed to shorter times available for carbide precipitation, leading to an overall softer matrix.

However, the overall limited effect suggests that the applied cooling rates were insufficient to induce substantial phase transformations towards martensite, which would otherwise drastically alter mechanical properties.

4.4. Conclusion

This study examined the influence of sintering temperature, atmosphere and PSD on density and hardness in AM samples presenting the complete BJT process chain. The key findings are:

- Density is maximized at elevated sintering temperatures, pressures, and under nitrogen atmospheres, with PSD playing a critical role in achieving near-full density.
- Hardness is primarily influenced by nitrogen-induced nitride formation and density, with a secondary dependence on cooling rate.
- Cooling rate and PSD exhibit complementary hardening effects, while holding time has a comparatively minor influence.

Further research will explore atmospheres like hydrogen or vacuum for HSS in BJT as these atmospheres are described to achieve higher densities [4]. Based on flexural strength analysis a sintering strategy for nitride formation to achieve surface hardening whilst avoiding brittle structure will be examined.

Acknowledgements

The authors would like to thank the Ministry of Science, Research and Arts of the Federal State of Baden-Württemberg for the financial support of the projects within the InnovationsCampus Future Mobility.

The authors further declare that they have no known competing financial interests or personal relationships that could have appeared to influence the work reported in this paper.

References

[1] Mostafaei A, De Vecchis PR, Kimes KA, Elhassid D, Chmielus M. Effect of binder saturation and drying time on microstructure and resulting properties of sinter-HIP binder-jet 3D-printed WC-Co composites. Additive Manufacturing 2021;46:102128.
[2] Chede SJ, Chopra MK, Dhokey NB, Aher VS, Ghosh P. Performance analysis of cryoprocessed conventional HSS M2 drill and P/M HSS M3 TiN coated tap and its effect on the substructure. Materials Today: Proceedings 2022;65:396–400.
[3] Mostafaei A, Elliott AM, Barnes JE, Li F, Tan W, Cramer CL, et al. Binder jet 3D printing—Process parameters, materials, properties, modeling, and challenges. Progress in Materials Science 2021;119:100707.
[4] German RM, Bose A. Binder and Polymer Assisted Powder Processing. Russel Township: ASM International; 2020.
[5] Kearns MA, Murray K, Davies PA, Ryabinin V, Gonzalez E. Sintering and properties of MIM M2 high speed steel produced by prealloy and master alloy routes. Metal Powder Report 2016;71(3):200–6.
[6] Asgharzadeh H, Simchi A. Effect of sintering atmosphere and carbon content on the densification and microstructure of laser-sintered M2 high-speed steel powder. Materials Science and Engineering: A 2005;403(1–2):290–8.
[7] Liu ZY, Loh NH, Khor KA, Tor SB. Sintering of injection molded M2 high-speed steel. Materials Letters 2000;45(1):32–8.
[8] Eroglu S. Sintering and Mechanical Properties of AISI M2 High-Speed Steel Powder Molded at Low Pressures. Materials and Manufacturing Processes 2010;25(9):1025–9.
[9] Anoop FR, Abraham Jacob B, Kuriachen B, Malgave S. Effect of heat treatment on microstructure and wear properties on Binder Jetting Additive manufactured M2 High-Speed steel. Materials Letters. 2024;375:137228.
[10] Choudhari A, Elder J, Mugale M, Karki S, Vukkum VB, Gupta RK, et al. Additive manufacturing of AISI M2 tool steel by binder jetting (BJ): Investigation of microstructural and mechanical properties. Journal of Manufacturing Processes. 2024;132:686–711.
[11] Choudhari A, Elder J, Mugale M, Karki S, Digole S, Omeike S, et al. Enhancing Quality Control: Image-Based Quantification of Carbides and Defect Remediation in Binder Jetting Additive Manufacturing. Materials. 2024;17(10):2174.
[12] Mirzababaei S, Paul BK, Pasebani S. Metal Powder Recyclability in Binder Jet Additive Manufacturing. JOM 2020;72(9):3070–9.
[13] E04 Committee. Guide for Preparation of Metallographic Specimens (E3-11). ASTM International; 2017.
[14] Subcommittee F42.01. Additive Manufacturing of Metal - Finished Part Properties - Methods for Relative Density Measurement (F3637-23). ASTM International; 2023.
[15] E04 Committee. Test Method for Microindentation Hardness of Materials (E384−22). ASTM International; 2022.